ELSEVIER

Surface Science 496 (2002) 238–250

SURFACE SCIENCE

www.elsevier.com/locate/susc

Crystal truncation rod diffraction study of the α-Al_2O_3 $(1\,\bar{1}\,0\,2)$ surface

Thomas P. Trainor [a,*], Peter J. Eng [b], Gordon E. Brown Jr. [a,c], Ian K. Robinson [d], Maurizio De Santis [e]

[a] *Department of Geological and Environmental Sciences, Stanford University, Stanford, CA 94305, USA*
[b] *Consortium for Advanced Radiation Sources and the James Franck Institute, University of Chicago, Chicago, IL 60637, USA*
[c] *Stanford Synchrotron Radiation Laboratory, SLAC, Stanford University, Stanford, CA 94025, USA*
[d] *Department of Physics, University of Illinois at Urbana-Champaign, Urbana, IL 61801, USA*
[e] *Laboratoire de Cristallographie, CNRS, B. P. 166, 38042 Grenoble, France*

Received 18 June 2001; accepted for publication 11 September 2001

Abstract

The structure of the α-Al_2O_3 $(1\,{-}1\,0\,2)$ surface was examined using crystal truncation rod (CTR) diffraction. The initial surface was prepared by Ar-ion sputter and anneal cycles in O_2, which resulted in a clean (1×1) surface. CTR data were then collected for the clean and water-dosed surfaces (1×10^{-8}–1.6 Torr) in a UHV diffraction chamber (base pressure ≈ 1–3×10^{-9} Torr). Water dosing had little effect on the diffraction data, suggesting that the initially prepared surface was fully oxygenated. Least-squares analysis of the CTR data resulted in two best fit models, a relaxed stoichiometric bulk termination and a relaxed bulk termination with a zero occupancy for the first layer of aluminum atoms. Crystal chemistry considerations suggest that the second model is the most plausible if the surface oxygens are protonated.

Keywords: X-ray scattering, diffraction, and reflection; Surface structure, morphology, roughness, and topography; Aluminum oxide

1. Introduction

Aluminum-oxide and hydroxide surfaces play an important role in a variety of fields including heterogeneous catalysis, thin film growth, corrosion, and aqueous and surface geochemistry. Single crystal and powdered substrates of α-Al_2O_3 are widely used as model systems for studying surface reactions of importance to these fields (cf. [1,2]). The energetics of reactions occurring at metal oxide surfaces are a function of both the surface composition and surface structure, which depend to a large extent on the sample history and environment. One of the key issues to be considered is the interaction of water with oxide surfaces and the resulting hydration or hydroxylation of the surfaces. The structures of hydrated oxide surfaces and the resulting surface structural changes are key in determining the surface reactivity in "wet" systems such as encountered in catalysis, aqueous

* Corresponding author. Address: Consortium for Advanced Radiation Sources, The University of Chicago, Building 434-A, 9700 South Cass Avenue, Argonne, IL 60439, USA. Tel.: +1-630-252-0433; fax: +1-630-252-0436.
E-mail address: trainor@cars.uchicago.edu (T.P. Trainor).

0039-6028/01/$ - see front matter
PII: S0039-6028(01)01617-X

geochemistry, and corrosion. However, detailed knowledge of oxide surface structures is limited, particularly for hydrated systems.

In this work we have examined the structure of the "clean" and water-exposed α-Al_2O_3 $(1\,-1\,0\,2)$ surface (*R*-plane) using crystal truncation rod (CTR) scattering. The primary reason for choosing this surface is its importance as a model for naturally abundant aluminum-(hydr)oxide phases, such as gibbsite and the aluminol layer of clay minerals, where the exposed surface sites are postulated to have similar local structure and reactivity. Further, this work extends our recent CTR study of the structure of the hydrated α-Al_2O_3 $(0\,0\,0\,1)$ surface (*C*-plane) which showed that significant relaxation accompanied hydration [3]. The application of CTR scattering to oxide surface structure determination has several advantages over traditional surface science techniques. Principally, CTR diffraction does not require the use of conducting substrates and can be performed under UHV conditions, in air, or in the presence of bulk solution (cf. [4]). The sensitivity of this technique for the determination of surface terminations, relaxations and reconstructions has been shown for a number of systems [5–7]. However, this diffraction technique requires high quality crystalline surfaces, of low surface roughness, and is only sensitive to structures with long-range order.

The structures of the clean and hydroxylated alumina surfaces, particularly the $(0\,0\,0\,1)$ surface, have been the subject of numerous experimental [3,8–12] and theoretical [13–21] studies. Several studies suggest that the clean $(0\,0\,0\,1)$ surface is terminated by a single aluminum layer, which leads to a stoichiometric, charge-neutral surface [8,9]. The terminating aluminum atoms are 3-fold coordinated by the underlying closest-packed oxygens and are significantly relaxed towards the bulk (cf. [13,18]). The 3-coordinate aluminum atoms are expected to be reactive towards basic species (e.g., water) due to their low coordination number, as observed in several studies [17,22–24]. We recently examined the structure of the fully hydrated $(0\,0\,0\,1)$ surface and found, in contrast with the clean surface structure, that the hydrated surface is hydroxyl terminated with a double aluminum layer below the terminating oxygen plane [3]. Further, there is a significant relaxation resulting in a surface layer resembling an intermediate between the bulk oxygen termination and that of γ-$Al(OH)_3$. The terminating surface oxygen atoms are 2-coordinated by Al, whereas all the aluminum atoms in the surface model are 6-coordinated.

The expected structure of the α-Al_2O_3 $(1\,-1\,0\,2)$ surface termination represents a significant contrast to the $(0\,0\,0\,1)$ surface. The stoichiometric bulk termination of the $(1\,-1\,0\,2)$ surface is expected to have 5-coordinated aluminum and 3-coordinated oxygen at the surface [21,25]. While the clean $(1\,-1\,0\,2)$ surface was also observed to be highly reactive to water [26], it is not clear that there should be a significant difference between the structure of the clean and hydrated surfaces due to the higher coordination of near-surface aluminum atoms in this model.

Further, it has been observed that there are significant differences in the reactivity of the hydrated $(0\,0\,0\,1)$ and $(1\,-1\,0\,2)$ α-Al_2O_3 surfaces towards aqueous Pb(II) [27–29], as well as differences in metal film growth depending on the preparation of the surfaces [30–32]. Therefore, our investigation of the surface structure of the $(1\,-1\,0\,2)$ α-Al_2O_3 surface after cleaning in UHV and water dosing is intended to provide some insight into the structural details which may help explain the differences in reactivity of these surfaces.

2. Bulk structure and surface unit cell

The structure of α-Al_2O_3 (space group $R\bar{3}c$) consists of distorted hexagonally closest packed layers of oxygen with aluminum occupying two thirds of the octahedral holes. The oxygen stacking sequence runs along the *c*-axis, and a unit cell contains six oxygen layers, giving six formula units per cell. The aluminum atoms are staggered along the *c*-axis from their ideal position centered between the oxygen layers. This leads to two sets of Al–O bond lengths. The aluminum that is displaced in the positive direction along the *c*-axis has three short Al–O bonds (1.86 Å) to the oxygen layer above and three long Al–O bonds (1.97 Å) to the oxygen layer below. This is reversed for the

aluminum atoms that are displaced in the negative direction along the c-axis. The cell parameters used in our work are from Kirfel and Eichhorn [33] ($|\mathbf{a}| = 4.757$ Å, $|\mathbf{c}| = 12.988$ Å) with bulk isotropic Debye–Waller factors from Ishizawa et al. [34].

The $(1\,-1\,0\,2)$ surface is characterized by a rectangular surface net as depicted in Fig. 1A. The (1×1) unit cell as defined in this work has in-plane lattice parameters [1] of $|\mathbf{a}_s| = 4.757$ Å, $|\mathbf{b}_s| = 5.127$ Å with $\mathbf{a}_s$ defined by the [1 1 0] vector and $\mathbf{b}_s$ defined by the [−1/3 1/3 1/3] vector in the bulk indexing ($\mathbf{b}_s$ is parallel to the projection of the c-axis onto the $(1\,-1\,0\,2)$ plane). Normal to the surface we have chosen $|\mathbf{c}_s| = 6.957$ Å ($2 \times d_{(1\,-1\,2)}$) which gives a cell containing 20 atoms (4 Al_2O_3 units) as shown in Fig. 1B. This cell has two structurally identical $(Al_2O_3)_2$ units with a linear shift of the atomic coordinates by half a lattice spacing along the $\mathbf{a}_s$ and $\mathbf{c}_s$ basis vectors and by $0.5 - \Delta/2$ ($\Delta = 0.1391$) along the $\mathbf{b}_s$ basis vector between the two units (see Table 1). The relevant layer spacings along the $\mathbf{c}_s$-axis are depicted in Fig. 1B.

The unit cell as defined above cannot be used as a space-filling model to generate the bulk α-Al_2O_3 structure by repeat along simple lattice vectors. For the case of the $(1\,-1\,0\,2)$ surface there exists no crystallographic unit cell that defines the bulk structure with two basis vectors in the surface plane and a third normal to the surface, as is conventionally used in surface scattering experiments. The cell defined above contains the correct repeat of atomic coordinates along the $\mathbf{a}_s$ and $\mathbf{c}_s$ basis, but for each cell repeat along the surface normal there is a shift of atomic coordinates along the $\mathbf{b}_s$ basis vector by $0.1391 n_3$ ($n_3 \leqslant 0$). Therefore, our definition of the unit cell in the surface indexing results in a pseudo-cell useful for calculating in-plane and surface normal relations but is not a crystallographic unit cell. However, the bulk structure can be generated from this pseudo-cell by applying a non-normal repeat vector. Defining the origin of the structure at the center of the surface plane, the coordinates of atom j in cell (n_1, n_2, n_3) are given by the vector

$$\mathbf{R}_j = \mathbf{r}_j(n_{1,2,3} = 0) + \mathbf{R}_s(n_{1,2}) + \mathbf{V}_r \tag{1}$$

where n is integer ($n_3 \leqslant 0$) and $\mathbf{r}_j$ $(n_{1,2,3} = 0)$ gives the fractional coordinates of atom j in the cell defining the origin. The vector $\mathbf{R}_s$ gives the in-plane coordinates for the origin of cell (n_1, n_2) in the n_3th slab,

$$\mathbf{R}_s(n_{1,2}) = n_1\mathbf{a}_s + n_2\mathbf{b}_s \tag{2}$$

and the vector $\mathbf{V}_r$ is the slab repeat vector giving the origin of cell $(n_{1,2} = 0, n_3)$,

$$\mathbf{V}_r = n_3\Delta\mathbf{b}_s + n_3\mathbf{c}_s \tag{3}$$

as shown in Fig. 1C. For our definition of the unit cell in the surface indexing, the parameter Δ has a value of 0.1391.

The indexing of the unit cell as above has the advantage that the reciprocal lattice is simply defined in terms of the surface termination since we base the reciprocal lattice on the definition of the unit cell real-space basis vectors. Therefore, the indices H_s and K_s give the degree of momentum transfer in the surface plane and L_s gives the degree of momentum transfer along the surface normal. The reciprocal lattice indices can be transformed from the bulk to the surface indexing using the transformation matrix,

$$\begin{pmatrix} H_s \\ K_s \\ L_s \end{pmatrix} = \begin{pmatrix} 1 & 1 & 0 \\ -1/3 & 1/3 & 1/3 \\ 0.713 & -0.713 & 0.287 \end{pmatrix} \begin{pmatrix} H \\ K \\ L \end{pmatrix} \tag{4}$$

and the reciprocal relation is given using the inverse of the transformation matrix.

The unit cell defined above results in a surface termination which is stoichiometric (i.e. charge neutral) with 5-fold coordinate aluminums and 3-fold coordinate oxygens at the surface (Fig. 1). This model is referred to below as the bulk-stoichiometric termination. The "zig-zag" rows of first-layer 3-coordinate oxygen and third-layer 4-coordinate oxygen run parallel to the $\mathbf{b}_s$ lattice vector. Other possible terminations can be envisioned by removing atomic layers within in the unit cell (e.g., removing the top oxygen layer results in an aluminum termination in which the

[1] We use $\mathbf{a}_s$, $\mathbf{b}_s$, $\mathbf{c}_s$ and H_s, K_s, L_s to refer, respectively, to the real-space basis vectors and reciprocal lattice indices in the surface indexing.

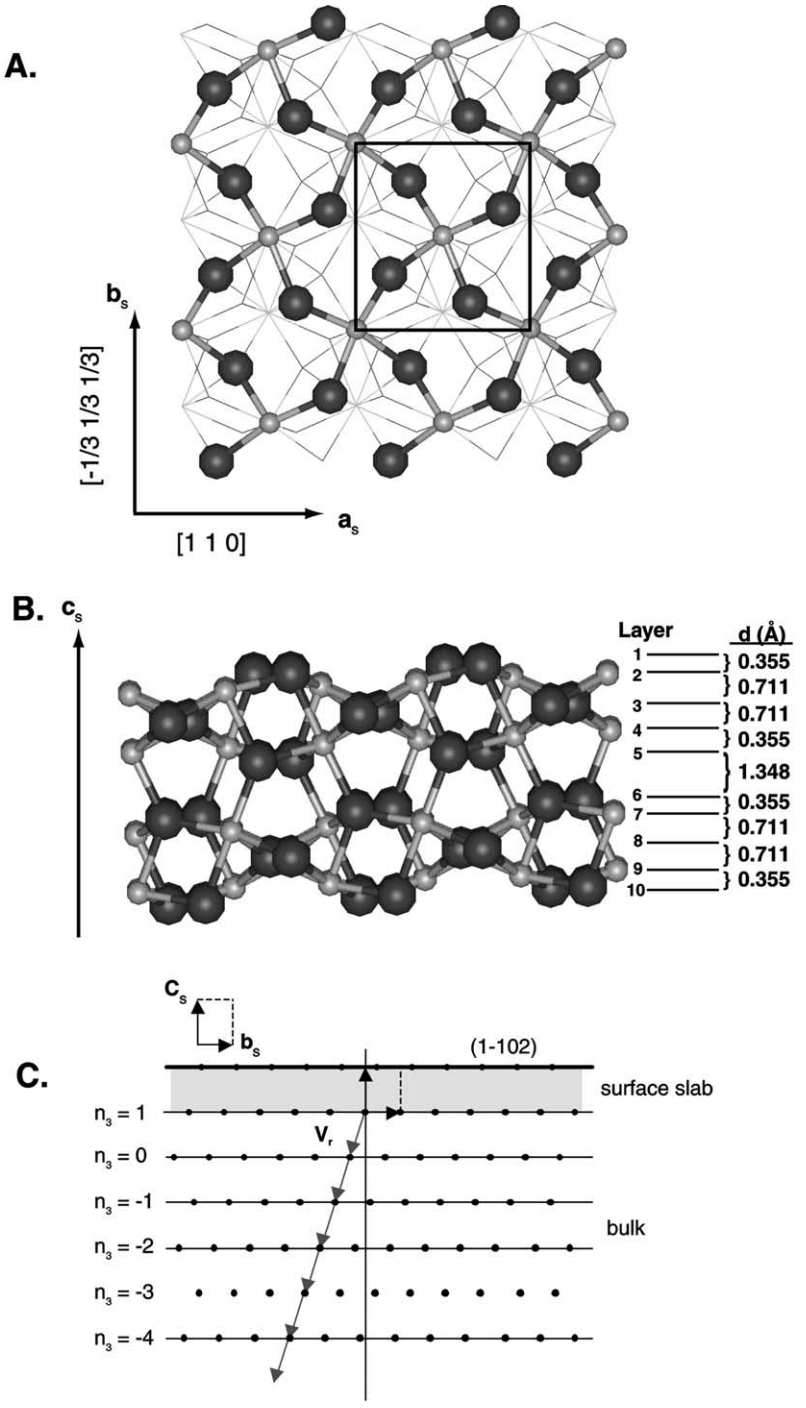

Fig. 1. Model of the ideal stoichiometric bulk termination of α-Al_2O_3 (1 −1 0 2). Large circles are oxygen small circles are aluminum. (A) In-plane view of the (1 −1 0 2) surface showing the surface net. The real-space basis vectors in the surface indexing are shown, along with their corresponding indices in the bulk indexing. (B) Layer stacking sequence and layer spacings along the $\mathbf{c}_s$-axis. (C) Schematic of the stacking sequence of the 2-D slabs along the surface normal, showing the definition of the slab repeat vector.

Table 1
Atomic fractional coordinates used for bulk cell

	x	y	z
O	0.653	0.833	0.903
O	0.847	0.333	0.903
Al	0.000	0.684	0.852
Al	0.500	0.184	0.852
O	0.194	0.965	0.750
O	0.306	0.465	0.750
Al	0.000	0.247	0.648
Al	0.500	0.747	0.648
O	0.653	0.097	0.597
O	0.847	0.597	0.597
O	0.153	0.264	0.403
O	0.347	0.764	0.403
Al	0.500	0.114	0.352
Al	0.000	0.614	0.352
O	0.694	0.396	0.250
O	0.806	0.896	0.250
Al	0.500	0.677	0.148
Al	0.000	0.177	0.148
O	0.153	0.528	0.097
O	0.347	0.028	0.097

The cell parameters are $|\mathbf{a}_s| = 4.7570$, $|\mathbf{b}_s| = 5.12692$, $|\mathbf{c}_s| = 6.9575$ and $\alpha = \beta = \gamma = 90°$.

aluminum is 4-fold coordinated). After five atomic layers, the structure of the surface terminations are chemically equivalent to the terminations in the top five layers, though the atomic coordinates are shifted as mentioned above.

3. Experimental

3.1. Sample preparation

A highly polished single crystal α-Al_2O_3 substrate of the $(1\,{-}1\,0\,2)$ orientation (0.5 mm thick) obtained from Union Carbide Crystal Products was used for the CTR measurements. The wafer was cut to ≈1 in. square and prepared with a mild acid etch (0.01 M HNO_3) followed by multiple rinses with MilliQ water and heating to 350 °C in air. After the sample had cooled to room temperature it was immediately subjected to an extensive wash with MilliQ water and blown dry with an Ar jet. Following this wash procedure, the sample was introduced into a UHV-diffraction chamber at the National Synchrotron Light Source (NSLS) beamline X16A [35,36] for further surface preparation and collection of CTR data.

The clean surface was prepared by annealing the sample to ≈900 °C in 1×10^{-6} Torr O_2 for 1 h followed by Ar-ion sputtering ($P_{Ar} = 5 \times 10^{-5}$ Torr, $E = 1$ keV) for 30 min. The sample was then annealed to 750 °C in 2×10^{-6} Torr O_2 for 1 h and a second anneal to ≈1000 °C for 1 h. The resulting surface displayed a sharp (1×1) LEED pattern and was free of carbon contamination as determined by Auger electron spectroscopy (less than 1% ML).

Water doses of increasing pressure, from 1×10^{-8}–1.6 Torr, were performed using a precision leak valve. The water used was from a MilliQ system (18 MΩ cm) and was degassed by several freeze–pump–thaw cycles under vacuum. Water exposures up to 1×10^{-6} Torr were carried out in the main UHV chamber, and water pressure was monitored with an ion-gauge. For the highest water dose, the sample was moved into a load lock for dosing where water pressure was monitored with a convectron gauge. Base pressure in the main chamber was $\approx 5 \times 10^{-10}$ Torr; however, after sample cleaning, the main chamber base pressure was ≈ 1–3×10^{-9} Torr and the chamber pressure would rapidly return to this range after water dosing.

3.2. Data collection

CTR data were collected using 9.3 keV X-rays collimated to 0.5×3 mm^2. Each data point consists of a rocking scan of the diffractometer ϕ-axis at the particular $[H_s, K_s, L_s]$ setting. Data were collected with both the incident and exit angles greater than the critical angle for total external reflection. The integrated, background-subtracted intensity for each value of the perpendicular momentum transfer was corrected for active area, polarization, step size and Lorentz factor [5]. The CTR data for the clean and water-dosed surface are shown in Fig. 2.

3.3. Data analysis

Data analysis was carried out using a non-linear least-squares routine with fixed bulk and

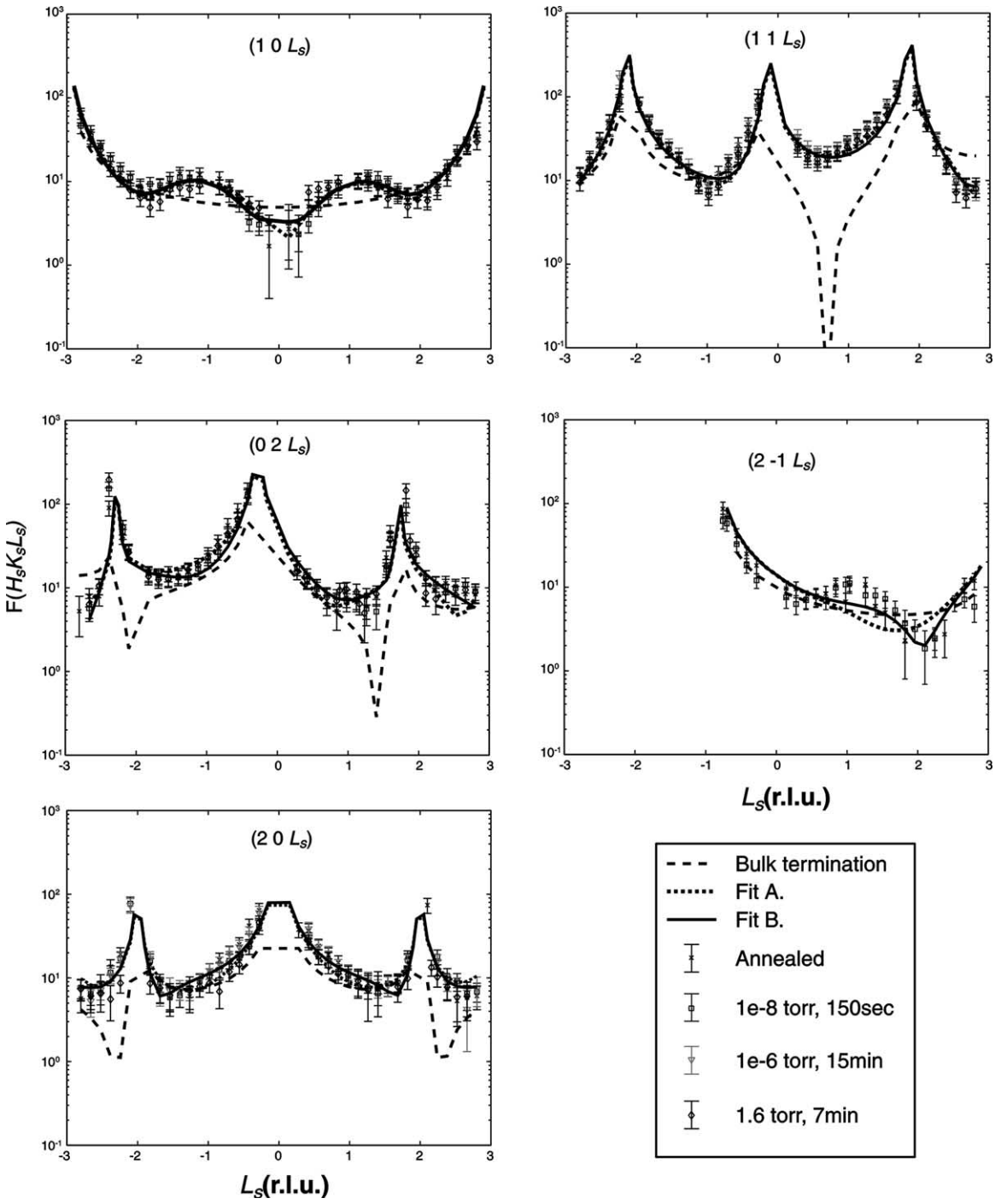

Fig. 2. Experimental structure factors (F_{HKL}) measured for the clean and water dosed α-Al_2O_3 (1 −1 0 2) surface as a function of perpendicular momentum transfer (L_s in reciprocal lattice units). The dashed line is the calculated CTR for the ideal termination, the dotted line is the best fit model A termination and the solid line is the best fit model B termination.

adjustable surface models. The calculation of CTR intensity was performed following the method outlined previously [37–39]. However, a slight modification was needed due to our choice of a non-crystallographic unit cell. The details of the method are given elsewhere [40,41], but the final result is arrived at by including the non-normal slab repeat vector (Eqs. (1)–(3)) in the derivation of the total structure factor.

The coordinates used in the bulk model are given in Table 1, and the surface model atomic coordinates are given in Table 2. For the particular case investigated here, the surface cell ($n_3 = 1$) has a difference in fractional coordinates from the bulk cell at ($n_{1,2,3} = 0$) by $y_s = y + \Delta$, where $\Delta = 0.1391$. In addition, we observed that within our surface cell there are two layers that will give chemically equivalent terminations. Therefore, for each termination investigated we included two surface models, one that was half the unit cell and the other the full unit cell, with the same variable model parameters for each. The magnitudes of the structure factors for the two surface models were summed to give the final calculated structure factor values. This model was used in the least-squares routine to minimize the χ^2 value as a function of the structural parameters.

As a check on the chemical plausibility of our models, we calculated the bond-valence sums for the atoms in the surface cell. Based on Pauling's electrostatic valence principle, the sum of the bond valence (s) contributions (where s is given by the ratio of the valence (z) to the coordination number of the ion) from each nearest-neighbor cation (anion) should equal the magnitude of the valence of the central anion (cation) [42]. This concept has been extended to include variations in bond valences as a function of bond length [43,44]. The values presented in Table 2 were calculated based on the empirical formulation of the bond length–bond strength relationship for metal oxides of Brown and Altermatt [44]. The bond valence sums for bulk oxygen and aluminum atoms in α-Al_2O_3 are calculated to be 2.0 valence units (v.u.) and 3.0 v.u., respectively. A bond valence sum lower than the formal valence (undersaturation) is a result of under-coordination or longer than expected bond lengths, while a bond valence sum of greater than the formal valence (oversaturation) indicates bond lengths are shorter than typically found in bulk oxide materials.

4. Results

Qualitative inspection of the rod profiles in Fig. 2 shows there is no significant variation as a function of the water dosing. After the cleaning procedure, the surface displayed a sharp (1×1) LEED pattern, and after the highest water dose, the LEED was of similar quality (still (1×1)) with an increase in the diffuse background. These observations imply that the water dosing did not significantly perturb the structure of the initially prepared crystalline surface. Because the rod profiles were reproducible throughout the water dosing series, final fits were carried out on all data simultaneously. Fits performed on individual data sets gave similar results as fits to the full data set.

The calculated CTRs for the un-relaxed bulk-stoichiometric termination are shown in Fig. 2 as the dashed line. It is apparent that the bulk-stoichiometric termination does not reproduce the data set, in particular the features at ± 1 on the $(10L_s)$ rod and the increase in the magnitude of the structure factor along the $(11L_s)$ rod between 0 and $\approx$1.9 r.l.u.

Least-squares fits of the full data set to models with various chemical terminations allowing relaxation of the atomic positions from the bulk positions were performed in the analysis procedure. The primary free variables in the fits are the atomic z-fractional coordinates, occupancies and Debye–Waller factors, as well as, overall roughness and scale factors. To reduce the number of free parameters in the fitting procedure we constrained the atoms in each layer to maintain the same z-coordinate, occupation and Debye–Waller factors. Furthermore, we note that in the bulk termination model (Fig. 1A) the layer 1 and layer 3 oxygen atoms form a tilted equatorial plane around the layer 2 aluminum atoms with a pseudo 4-fold symmetry [45]. Therefore, to further reduce the number of free parameters, the in-plane displacements of the equatorial oxygen atoms were constrained, using a single displacement vector, to

Table 2
Best fit model parameters and estimated errors from the least-squares fits (96% confidence interval)

Layer		Un-relaxed			Model A						
		x	y	z	x	y	z	Δz (Å)	B_{iso} (Å^2)	Occ	$\sum s$
1	O	0.653	0.973	1.903	0.664(3)	0.990(3)	1.884(6)	−0.13(4)	9(4)	0.54(6)	1.73(5)
	O	0.847	0.473	1.903	0.827(3)	0.481(3)	1.884(6)	−0.13(4)	9(4)	0.54(6)	1.75(4)
2	Al	0.000	0.823	1.852	0.000	0.823	1.880(6)	0.19(4)	10(4)	0.43(8)	1.96(2)
	Al	0.500	0.323	1.852	0.500	0.323	1.880(6)	0.19(4)	10(4)	0.43(8)	2.20(2)
3	O	0.194	0.104	1.750	0.211(3)	0.092(3)	1.712(4)	−0.26(3)	0.33	1	1.84(2)
	O	0.306	0.604	1.750	0.293(3)	0.589(3)	1.712(4)	−0.26(3)	0.33	1	1.83(2)
4	Al	0.000	0.386	1.648	0.000	0.386	1.651(3)	0.02(2)	0.32	1	3.4(1)
	Al	0.500	0.886	1.648	0.500	0.886	1.651(3)	0.02(2)	0.32	1	3.4(1)
5	O	0.653	0.236	1.597	0.653	0.236	1.605(3)	0.05(2)	0.33	1	1.9(1)
	O	0.847	0.736	1.597	0.847	0.736	1.605(3)	0.05(2)	0.33	1	1.9(1)
6	O	0.153	0.403	1.403	0.153	0.403	1.408(3)	0.04(2)	0.33	1	1.99(4)
	O	0.347	0.903	1.403	0.347	0.903	1.408(3)	0.04(2)	0.33	1	1.99(4)
7	Al	0.500	0.253	1.352	0.500	0.253	1.361(2)	0.06(1)	0.32	1	2.86(6)
	Al	0.000	0.753	1.352	0.000	0.753	1.361(2)	0.06(1)	0.32	1	2.86(6)
8	O	0.694	0.535	1.250	0.694	0.535	1.243(2)	−0.05(2)	0.33	1	1.94(3)
	O	0.806	0.035	1.250	0.806	0.035	1.243(2)	−0.05(2)	0.33	1	1.94(3)
9	Al	0.500	0.816	1.148	0.500	0.816	1.148	0	0.32	1	3.01(7)
	Al	0.000	0.316	1.148	0.000	0.316	1.148	0	0.32	1	3.01(7)
10	O	0.153	0.667	1.097	0.153	0.667	1.097	0	0.33	1	1.94(3)
	O	0.347	0.167	1.097	0.347	0.167	1.097	0	0.33	1	1.94(3)
					Model B						
1	O	0.653	0.973	1.903	0.72(2)	0.84(2)	1.91(2)	0.1(1)	20(5)	0.7(1)	0.3(2)
	O	0.847	0.473	1.903	0.78(2)	0.34(2)	1.91(2)	0.1(1)	20(5)	0.7(1)	0.3(2)
2	Al	0.000	0.823	1.852							
	Al	0.500	0.323	1.852							
3	O	0.194	0.104	1.750	0.177(4)	0.086(4)	1.703(7)	−0.33(5)	3(2)	0.9(1)	1.22(2)
	O	0.306	0.604	1.750	0.328(4)	0.591(4)	1.703(7)	−0.33(5)	3(2)	0.9(1)	1.24(2)
4	Al	0.000	0.386	1.648	0.000	0.386	1.650(4)	0.01(3)	8(2)	1	3.0(3)
	Al	0.500	0.886	1.648	0.500	0.886	1.650(4)	0.01(3)	8(2)	1	3.0(3)
5	O	0.653	0.236	1.597	0.636(4)	0.254(4)	1.583(5)	−0.10(3)	0.33	1	1.64(3)
	O	0.847	0.736	1.597	0.867(4)	0.752(4)	1.583(5)	−0.10(3)	0.33	1	1.65(4)
6	O	0.153	0.403	1.403	0.153	0.403	1.411(4)	0.05(3)	0.33	1	1.98(3)
	O	0.347	0.903	1.403	0.347	0.903	1.411(4)	0.05(3)	0.33	1	1.98(3)
7	Al	0.500	0.253	1.352	0.500	0.253	1.353(3)	0.00(2)	0.32	1	3.15(8)
	Al	0.000	0.753	1.352	0.000	0.753	1.353(3)	0.00(2)	0.32	1	3.16(9)
8	O	0.694	0.535	1.250	0.694	0.535	1.241(3)	−0.07(2)	0.33	1	2.00
	O	0.806	0.035	1.250	0.806	0.035	1.241(3)	−0.07(2)	0.33	1	2.00
9	Al	0.500	0.816	1.148	0.500	0.816	1.148(3)	0.00(2)	0.32	1	3.02(8)
	Al	0.000	0.316	1.148	0.000	0.316	1.148(3)	0.00(2)	0.32	1	3.02(8)
10	O	0.153	0.667	1.097	0.153	0.667	1.099(3)	0.01(2)	0.33	1	1.99(5)
	O	0.347	0.167	1.097	0.347	0.167	1.099(3)	0.01(2)	0.33	1	1.99(5)

Values without reported errors were held fixed in the final fits. The Δz values are the change in the layer z position with respect to the perfect termination. Bond valence sums ($\sum s$) were calculated assuming unit site occupancies.

maintain the approximate 4-fold symmetry of the in-plane projections of the oxygen atoms. As a result, the atoms are forced to rotate and breath as a group. Other constraint sets are possible, such as those that allow rumpling of the surface. However, we could obtain reasonable quality fits of the data within our set of constraints using a minimum of free parameters.

Each of the five potential (1×1) chemical terminations was examined in the analysis procedure.

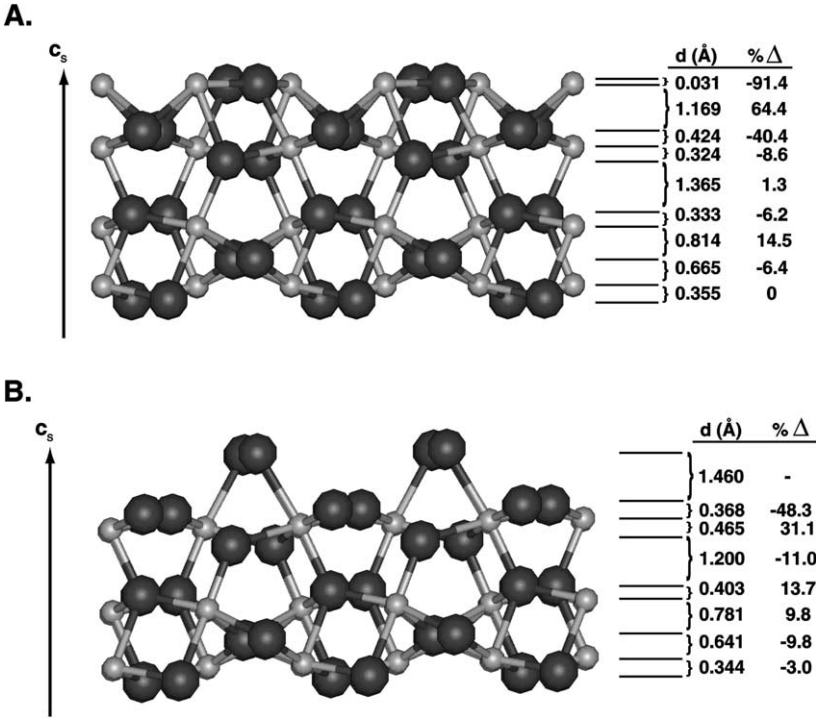

Fig. 3. Atomic layer sequence and layer spacings of the best fit surface models from analysis of CTR data. Large circles are oxygen small circles are aluminum. (A) Model A is relaxed bulk termination. (B) Model B is relaxed termination with zero occupancy for layer 2 aluminum. $\%\Delta$ is the percent change in the layer spacing from the ideal (unrelaxed) termination.

Two models were found that could reasonably reproduce the measured rod profiles (Fig. 3). Model A, a relaxed bulk-stoichiometric termination, and model B, a layer 3 termination with adsorbed O_2 or water residing in the layer 1 lattice positions, are discussed further below.

Allowing relaxation of the bulk-stoichiometric termination resulted in the fit shown as the dotted line in Fig. 2 with the ball and stick model depicted in Fig. 3A (model A). The fit resulted in a χ^2 value of 1.72 with the resulting fit parameters given in Table 2. The fit given by the relaxed bulk termination (model A) reproduces the majority of features of the rod set with the exception of the broad feature at $L_s \approx 1$ on the (2–1L_s) rod. The model resulting from this fit has large contraction of the layer 1–2 (−91%) and 3–4 (−40%) spacing and large expansion of the layer 2–3 (64%) spacing. The second-layer aluminum atoms move into nearly the same plane as the first layer oxygens, and there is a large contraction of the layer 3 oxygens (−0.26 Å) towards the bulk. The occupancies and Debye–Waller factors derived from the refinement for the first and second layer oxygen and aluminum, respectively, suggest that these first two layers of atoms have a high degree of disorder, though the refined value for the roughness parameter β [37] was approximately zero.

A second model based on a relaxed layer 3 termination was also found to give a good fit to the data set. The relaxed layer 3 termination resulted in a χ^2 value of 1.92, and also resulted in a large relaxation of the layer 3 oxygens (−0.33 Å) into the bulk. The fit was further improved by reintroducing the layer 1 oxygens ($\chi^2 = 1.6$, model B). This improvement was found to be statistically significant through application of the Hamilton R-ratio test [46], though the inclusion of this layer had little effect on the relaxation of atoms in layers 3 and below. Constraints similar to those mentioned above were applied in the fitting procedure for this model. The layer 3 and 4 oxygens were

constrained to maintain the approximate 4-fold symmetry of their in-plane projections, and the layer 1 oxygens (now singly coordinated with layer 3 Al) were constrained to have the same in-plane displacements.

The fit resulting in model B also shows a large contraction of the layer 3–4 (−48%) spacing as well as a large expansion of the layer 4–5 (31%) spacing. Further, the layer 1 oxygens have a large Debye–Waller factor and 0.7 occupancy, suggesting that this topmost layer of oxygens is significantly disordered. The fit resulted in a roughness parameter of $\beta = 0.18 \pm 0.03$ which gives an estimated rms surface roughness of <5 Å.

5. Discussion

5.1. Analysis of best fit models

Model B results in a slightly better χ^2 value than model A, with the largest qualitative difference in the fits being that model B appears to better reproduce the hump on the (2–1L_s) rod. The major structural difference in the two models is the presence or absence of the layer 2 aluminum atoms. In model A we found a 40% occupancy for the layer 2 aluminum with a contraction of layer 1 oxygen and expansion of layer 2 aluminum. Removing the layer 2 aluminum atoms results in an expansion and significant increase in the Debye–Waller factor of the layer 1 oxygen (model B). Based solely on χ^2 values, both models A and B are equally plausible. However, some distinction can be made based on the crystal chemical plausibility of the resulting structures, as discussed below.

In model A the relaxation results in the layer 1 oxygen and layer 2 aluminum residing in nearly a single plane. The bond lengths between the layer 1 oxygen and layer 2 aluminum remain in a reasonable range (∼1.75–1.94 Å). However, the large expansion of the layer 2 aluminum and contraction of the layer 3 oxygen leads to a large increase in the bond lengths between the layer 2 aluminum and layer 3 and 4 oxygen (2.05–2.18 Å). The average bond length of the second layer aluminum (2.01 Å) are longer than expected for 5- (or even 6-) coordinated aluminum and results in significant under-saturation (by ∼0.80–1.04 v.u.) of the layer 2 aluminum (Table 2). While we would expect the layer 2 aluminum to be undersaturated by ≈0.5 v.u. due to loss of its sixth neighbor, this should result in a decrease rather than an increase in the average bond length. Additional fits were attempted with the next layer of oxygen included in the model such that the layer 2 aluminum would be 6-coordinated. The inclusion of the additional oxygen atoms resulted in a small occupation factor, and the improvement in χ^2 was not statistically significant.

In model B the Al–O bond lengths remain in reasonable ranges, and the layer 4 aluminum are saturated due to the inclusion of the layer 1 oxygen. The layer 7 aluminum atoms are slightly oversaturated due to the shortening of the bonds to the layer 3 oxygen (to ∼1.73 Å) resulting from the large contraction of the layer 3 oxygen. However, the layer 1 oxygens are 1-coordinated with aluminum and therefore significantly under-saturated. Further, the 2-coordinate layer 3 oxygen and 3-coordinate layer 5 oxygen are undersaturated due to their under-coordination in the model. While the Al–O bond lengths and aluminum saturation indices in model B appear to be more reasonable than model A, the undersaturation of the surface oxygen and resulting non-stoichiometric surface are problematic.

The undersaturation of the surface oxygens and net excess of negative charge in model B is potentially relieved by proton binding. Nui et al. [31] observed that Ar ion sputtering at 1 keV on the α-Al_2O_3 (0 0 0 1) surface was insufficient to dehydroxylate the initial surface. Similarly, Ahn and Rabalais [9] found evidence for hydrogen on the (0 0 0 1) surface after annealing to temperatures of 1100 °C. Therefore, it appears likely that the cleaning procedure we followed, while sufficient to remove the majority of adventitious C, did not significantly dehydroxylate the surface. Furthermore, because of the large degree of disorder, partial occupancy and relatively large expansion (0.1 Å) of the layer 1 oxygen atoms included in model B, we suggest that the observation of oxygen atoms in layer 1 is due to the presence of adsorbed O_2 (from the O_2 anneal cycle) and/or water at the 5-coordinate aluminum sites. The atomic

positions of the layer 1 adsorbates are poorly constrained due to their relatively weak effect on the rod structure. Therefore, based on the above discussion it seems that the termination in model B results in a better surface model from the point of view of bond lengths and saturation of the surface atoms.

5.2. Comparison with previous work

Previous studies of the $(1\,-1\,0\,2)$ α-Al_2O_3 surface have reported both (1×1) and (1×2) surfaces depending on the preparation conditions. The stable reconstruction of this surface is reported to be (1×2) after sputtering and/or annealing to high temperature in UHV [25,26,32]. The reconstruction has been ascribed to ordered oxygen vacancies along the "zig-zag" rows parallel to the $\mathbf{b}_s$-axis. As mentioned above we did not observe any reconstruction in the LEED patterns after the sputter–anneal cycle. However, our preparation by low energy Ar-ion sputter and annealing treatment in O_2 is not expected to result in a high density of oxygen vacancies (c.f. [31]). In contrast, the more aggressive surface cleaning by previous authors (Ar-ion sputter at 5 keV and annealing in the absence of O_2) likely results in an oxygen deficient surface [25].

As mentioned above, the bulk cell (layer 1) termination is stoichiometric, leading to a surface with no net charge. If the reported (1×2) reconstruction is due to the presence of oxygen vacancies, it is noted that the reconstructed bulk termination would no longer be charge neutral since there would be an excess of positive charge in the surface layer. However, the layer 3 termination could result in a similar (1×2) termination, which is stoichiometric, by the presence of an ordered array of oxygen vacancies in layer 3. Therefore, we suggest that the layer 3 termination (with oxygen vacancies) is a possible candidate for the reconstructed surface due to its stoichiometric structure.

In the water sorption work of Schildbach and Hamza [26], they observe a rapid reaction of the (1×2) reconstructed surface (sticking coefficient of $\sim$0.8) with water up to $\approx$0.8 ML, then a significant reduction in sticking coefficient to $\sim$0.03 likely as a result of physisorbed molecular water. Much of the initially rapid uptake of water observed by Schildbach and Hamza was ascribed to healing of oxygen vacancies resulting from surface preparation. The reconstructed oxygen deficient surface would be expected to be highly reactive to water due to the presence of 4-coordinate aluminum atoms at the surface. Furthermore, undersaturated surface oxygens are expected to be highly reactive towards protons or other Lewis acid species. Therefore, water reaction would be expected to lead to the formation of terminal hydroxyl groups at under coordinated surface aluminum sites and to protonation of under coordinated oxygen atoms (c.f. [18]).

In comparing the expected results of water reaction on model A and model B, we observe that additional water sorption on the oxygenated surface should not lead to any significant structural changes since the near-surface aluminum atoms are already 6-fold coordinated. In contrast the surface aluminum atoms in model A should be reactive towards water due to their large undersaturation and would likely have resulted in some observable change in the rod structures based on simulations including an overlayer of oxygen (given a sufficiently large site occupancy). Therefore, we suggest that our surface preparation using lower energy Ar-ion sputter and annealing cycles in O_2 resulted in an oxygenated surface termination (model B) with the presence of hydrogen balancing the oxygen dangling bonds in layer 3 and the layer 1 oxygen are interpreted as adsorbed O_2 or water.

6. Conclusions

We conclude that the best model for interpretation of the CTR data on the $(1\,-1\,0\,2)$ surface is the relaxed layer 3 oxygen termination with partial occupancy of the layer 1 oxygen sites (model B). Both the very large relaxations in model A leading to unreasonable Al–O bond lengths and the lack of any significant structural changes upon water dosing suggest that relaxed bulk termination (model A) is the less plausible solution. Though model B is not stoichiometric (i.e., results in excess negative charge), the likely presence of residual

hydroxyls would decrease the net surface charge and saturate the dangling oxygen bonds. Further, we would expect that under more aggressive cleaning procedures resulting in an oxygen deficient surface, the likely model for the previously observed (1×2) reconstruction is a layer 3 termination with oxygen vacancies.

Our proposed model for the structure of the hydrated/oxygenated α-Al_2O_3 $(1\,-1\,0\,2)$ surface implies the presence of surface oxygens which are singly, triply and doubly coordinated with aluminum. In contrast, the structure of the fully hydrated $(0\,0\,0\,1)$ surface is terminated by only doubly coordinated surface oxygens. Differences in the coordination of surface oxygens have been used to interpret/predict the acid/base character (c.f. [47,48]) and reactivity of various terminating planes of a crystalline material [27,49]. As such, our results imply the previously observed differences in reactivity between the $(0\,0\,0\,1)$ and $(1\,-1\,0\,2)$ surfaces is likely a result of the variations in oxygen coordination of the surface functional groups.

Acknowledgements

We thank Alexis Templeton and Tom Kendelewicz for helpful discussions and comments. This work was carried out with support from the DOE through grant DE-FG03-93ER14347-A007 (Brown), DE-FG02-94ER14466 (Eng) and DE-FG02-96ER45439 (Robinson). Data collection was performed at the National Synchrotron Light Source (NSLS) which is supported through DOE grant DE-AC02-98CH10886.

References

[1] G.E. Brown Jr. et al., Chem. Rev. 99 (1999) 77–174.
[2] H. Knozinger, P. Ratnasamy, Catal. Rev. Sci. Eng. 17 (1978) 31–70.
[3] P.J. Eng, T.P. Trainor, G.E. Brown Jr., G.A. Waychunas, M. Newville, S.R. Sutton, M.L. Rivers, Science 288 (2000) 1029–1033.
[4] P. Fenter, P. Geissbühler, E. DiMasi, G. Srajer, L.B. Sorensen, N.C. Sturchio, Geochim. Cosmochim. Acta 64 (2000) 1221–1228.
[5] I.K. Robinson, in: G. Brown, D.E. Moncton (Eds.), Handbook on Synchrotron Radiation, Elsevier, Amsterdam, 1991, pp. 221–266.
[6] R. Feidenhans'l, Surf. Sci. Rep. 10 (1989) 105–188.
[7] G. Renaud, Surf. Sci. Rep. 32 (1998) 1–90.
[8] P. Guenard, G. Renaud, A. Barbier, M. Gautier-Soyer, Surf. Rev. Lett. 5 (1997) 321–324.
[9] J. Ahn, J.W. Rabalais, Surf. Sci. 388 (1997) 121–131.
[10] J. Toofan, P.R. Watson, Surf. Sci. 401 (1998) 162–172.
[11] M. Gautier, G. Renaud, L. Van Pham, B. Villette, M. Pollak, N. Thromat, F. Jollet, J.P. Duraud, J. Am. Ceram. Soc. 77 (1994) 323–334.
[12] M. Gillet, J.C. Bruna, Surf. Rev. Lett. 5 (1998) 325–329.
[13] X.-G. Wang, A. Chaka, M. Scheffler, Phys. Rev. Lett. 84 (2000) 3650–3653.
[14] R. Di Felice, J.E. Northrup, Phys. Rev. B 60 (1999) 16287–16290.
[15] A. Wander, B. Searle, N.M. Harrison, Surf. Sci. 458 (2000) 25–33.
[16] C. Verdozzi, D.R. Jennison, P.A. Schultz, M.P. Sears, Phys. Rev. Lett. 82 (1999) 799–802.
[17] K.C. Hass, W.F. Schneider, A. Curioni, W. Andreoni, Science 282 (1998) 265–268.
[18] K.C. Hass, W.F. Schneider, A. Curioni, W. Andreoni, J. Phys. Chem. B 104 (2000) 5527–5540.
[19] V.E. Puchin, J.D. Gale, A.L. Shluger, E.A. Kotomin, J. Guenster, M. Brause, V. Kempter, Surf. Sci. 370 (1997) 190–200.
[20] T.J. Godin, J.P. LaFemina, Phys. Rev. B 49 (1994) 7691–7696.
[21] J. Guo, D.E. Ellis, D.J. Lam, Phys. Rev. B 45 (1992) 13647–13656.
[22] P. Liu, T. Kendelewicz, G.E. Brown Jr., E.J. Nelson, S.A. Chambers, Surf. Sci. 417 (1998) 53–65.
[23] C.E. Nelson, J.W. Elam, M.A. Cameron, M.A. Tolbert, S.M. George, Surf. Sci. 416 (1998) 341–353.
[24] J.W. Elam, C.E. Nelson, M.A. Cameron, M.A. Tolbert, S.M. George, J. Phys. Chem. B 102 (1998) 7008–7015.
[25] E. Gillet, B. Ealet, Surf. Sci. 273 (1992) 427–436.
[26] M.A. Schildbach, A.V. Hamza, Surf. Sci. 282 (1993) 306–322.
[27] J.R. Bargar, S.N. Towle, G.E. Brown Jr., G.A. Parks, J. Colloid Interf. Sci. 185 (1997) 473–492.
[28] J.R. Bargar, S.N. Towle, G.E. Brown Jr., G.A. Parks, Geochim. Cosmochim. Acta 60 (1996) 3541–3547.
[29] A.S. Templeton, T.P. Trainor, S.J. Traina, A.M. Spormann, G.E. Brown Jr., Proc. Nat. Acad. Sci. 98 (2001) 11897–11902.
[30] J.A. Kelber, C. Niu, K. Shepherd, D.R. Jennison, A. Bogicevic, Surf. Sci. 446 (2000) 76–88.
[31] C. Niu, K. Shepherd, D. Martini, J. Tong, J.A. Kelber, D.R. Jennison, A. Bogicevic, Surf. Sci. 465 (2000) 163–176.
[32] M. Gillet, A.A. Mohammad, K. Masek, E. Gillet, Thin Solid Films 374 (2000) 134–141.
[33] A. Kirfel, K. Eichhorn, Acta Crystallogr. A 46 (1990) 271–284.

[34] N. Ishizawa, T. Miyata, I. Minato, F. Marumo, S. Iwai, Acta Crystallogr. B 36 (1980) 228–230.
[35] P.H. Fuoss, I.K. Robinson, Nucl. Instrum. Methods Phys. Res. A 222 (1984) 171–176.
[36] I.K. Robinson, in: E.N. Kaufmann (Ed.), Methods in Materials Research, Wiley, New York, 1999.
[37] I.K. Robinson, Phys. Rev. B 33 (1986) 3830–3836.
[38] E. Vlieg, J. Appl. Crystallogr. 33 (2000) 401–405.
[39] E. Vlieg, J.F. Van der Veen, S.J. Gurman, C. Norris, J.E. Macdonald, Surf. Sci. 210 (1989) 301–321.
[40] T.P. Trainor, P.J. Eng, I.K. Robinson, in preparation.
[41] T.P. Trainor, X-ray Scattering and X-ray Absorption Spectroscopy Studies of the Structure and Reactivity of Aluminum Oxide Surfaces, Thesis, Stanford University, Stanford, CA, 2001, p. 201.
[42] L. Pauling, The Nature of the Chemical Bond, third ed., Cornell University Press, Ithaca, New York, 1960.
[43] I.D. Brown, R.D. Shannon, Acta Crystallogr. A 29 (1973) 266–282.
[44] I.D. Brown, D. Altermatt, Acta Crystallogr. B 41 (1985) 244–247.
[45] C.C. Chang, J Vac. Sci. Tech. 8 (1971) 500–511.
[46] W.C. Hamilton, Acta. Cryst. 18 (1965) 502–510.
[47] T. Hiemstra, P. Venema, W.H. van Riemsdijk, J. Colloid Interf. Sci. 184 (1996) 680–692.
[48] J.R. Rustad, E. Wasserman, A.R. Felmy, Surf. Sci. 424 (1999) 28–35.
[49] J.D. Ostergren, T.P. Trainor, J.R. Bargar, G.E. Brown Jr., G.A. Parks, J. Colloid Interf. Sci. 225 (2000) 466–482.